

Compositional uniformity, domain patterning and the mechanism underlying nano-chessboard arrays

Santiago González¹, J.M. Perez-Mato^{1,*}, Luis Elcoro¹, Alberto García², Ray L. Withers³, and L. Bourgeois⁴

¹ *Departamento de Física de la Materia Condensada, Facultad de Ciencia y Tecnología, Universidad del País Vasco (UPV-EHU), Apdo. 644, 48080 Bilbao, Spain.*

² *Institut de Ciència de Materials de Barcelona, (ICMAB-CSIC), Campus de la UAB, E-08193 Bellaterra, Spain.*

³ *Research School of Chemistry, The Australian National University, Canberra, A.C.T, Australia and*

⁴ *Monash Centre for Electron Microscopy (MCEM), Monash University, Clayton, Victoria, Australia.*

(Dated: November 7, 2018)

We propose that systems exhibiting compositional patterning at the nanoscale, so far assumed to be due to some kind of ordered phase segregation, can be understood instead in terms of coherent, single phase ordering of minority motifs, caused by some constrained drive for uniformity. The essential features of this type of arrangements can be reproduced using a superspace construction typical of uniformity-driven orderings, which only requires the knowledge of the modulation vectors observed in the diffraction patterns. The idea is discussed in terms of a simple two dimensional lattice-gas model that simulates a binary system in which the dilution of the minority component is favored. This simple model already exhibits a hierarchy of arrangements similar to the experimentally observed nano-chessboard and nano-diamond patterns, which are described as occupational modulated structures with two independent modulation wave vectors and simple step-like occupation modulation functions.

PACS numbers: 61.50.Nw, 61.44.Fw, 62.23.Pq, 68.37.Lp

I. INTRODUCTION

Domain self-patterning on the nanoscale, particularly if the nanoscale chemical ordering can be engineered or tuned, is the goal of much research in the nanoscience and nanotechnology area. Potential applications include the use of the surfaces of such materials as templates for the assembly of molecular monolayers, for the reliable synthesis of functional nano-structured materials or for the structured adsorption of gas species. The recent discovery that tuneable nanoscale ordering occurs spontaneously in the wide range, non-stoichiometric $\text{Li}_{1/2-3x}\text{Ln}_{1/2+x}\text{TiO}_3$, $0.02 \leq x \leq 0.12$, solid solution¹ as well as in a variety of other A-site ordered perovskite-related phases^{2,3} is thus of intense current research interest. Guiton and Davies¹ demonstrated the existence of 2D, nanoscale compositional ordering in the $\text{Li}_{1/2-3x}\text{Nd}_{1/2+x}\text{TiO}_3$, $0.02 \leq x \leq 0.12$, system via High Angle Annular Dark Field (HAADF) imaging and interpreted this result in terms of phase segregation arising from some kind of “ordered” spinodal decomposition into $\text{Li}_{1/2}\text{Nd}_{1/2}\text{TiO}_3$ nano-chessboard regions separated by narrow $\text{Nd}_{2/3}\text{TiO}_3$ boundary regions. As an example, Fig. 1 shows the kind of nano-patterns that can be observed in this compound.

The 2D apparent phase separation into compositionally distinct areas described above is strongly reminiscent of the 1D atomic order that takes place in many compositionally flexible ordered phases. The list is very extensive, but one can cite for instance many binary and/or ternary alloy systems,⁴⁻⁶ reduced rutile structures such as the $\text{Ti}_n\text{O}_{2n-1}$ system,^{5,7} ReO_3 related compounds

such as the MoO_{3-x} system,⁸ the hexagonal perovskite related $\text{LaTi}_{1-x}\text{O}_3$ family⁹, the $(1-x)\text{Ta}_2\text{O}_5 + x\text{WO}_3$ system,^{10,11} and others.¹² In most of these 1D compositionally ordered arrangements, the basic driving mechanism is the maximization of the separation of *minority* structural motifs within a matrix of an underlying sub-structure. In the case of binary alloy systems, for example, there is usually a well-defined majority motif such as an ordered Cu_3Au unit which is, as regularly as possible, interleaved with a minority anti-phase boundary (APB) type structural motif, which locally has a different composition and leads to a continuously variable overall composition dependent upon the spatial distribution of the minority motif. Likewise, in the case of the reduced rutile $\text{Ti}_n\text{O}_{2n-1}$ system, the majority motif is the rutile type TiO_2 structure, while the minority motif is a crystallographic shear plane (CSP), which again changes the overall composition if “regularly” and uniformly arranged. These compositional orderings are one-dimensional and often yield patterns with composition varying in the nanoscale in the form of stripes (e.g. see Fig. 2).

In the last decade it has been shown^{9,12} that this type of one-dimensional uniformity-driven arrangement can be most efficiently described by means of step-like atomic occupation modulations with wave vectors and forms for the modulation functions that can be systematized according to simple rules using the superspace formalism.¹⁴⁻¹⁶ Very recently, the main ideas have been extended to the analysis of the distribution of minority motifs in *two-dimensional* systems,¹⁷ showing that pseudouniform arrangements can originate as the result of a simple quest for maximal dilution of a minority motif within lattice-

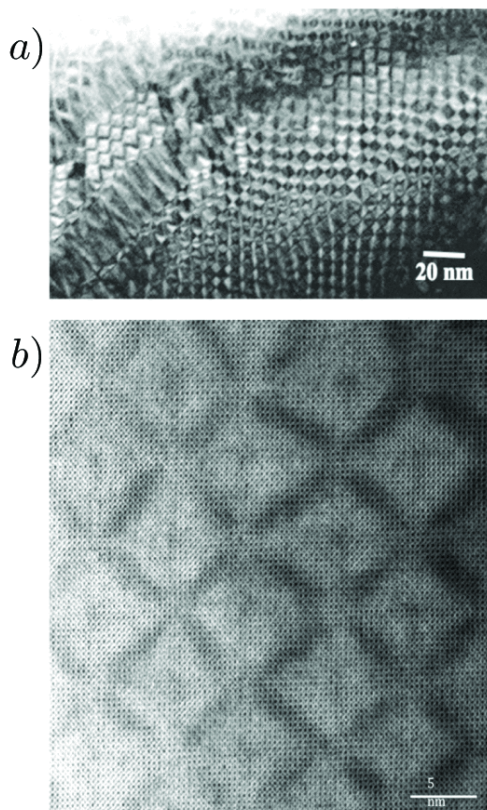


FIG. 1: (a) A typical low resolution TEM image of the chessboard type nano-structure characteristic of a $\text{Li}_{1/2-3x}\text{Nd}_{1/2+x}\text{TiO}_3$, $x=0.067$, sample. (b) a high resolution Bright Field STEM image of this nano-chessboard array. The lighter regions are Nd-poor and presumed to correspond to regions of stoichiometry $\text{Li}_{1/2}\text{Nd}_{1/2}\text{TiO}_3$ while the darker boundary regions are Nd-rich and presumed to correspond to the stoichiometry $\text{Nd}_{2/3}\text{TiO}_3$, according to Ref. 1.

restricted sites. In wide ranges of composition, the dilution drive was shown to stabilize 1D stripe arrangements oblique to the underlying lattice, following predictable rules based on the alternation of sub-units of different compositions on the nanoscale, but still keeping an overall identity as one single phase. The stripe arrangements were again shown to be easily describable as occupationally modulated structures, needing only a single modulation vector (as befits their intrinsic one-dimensionality) that can be determined unambiguously from the diffraction diagram of the system.

In this paper we show that these findings can be extended to the case of intrinsically two-dimensional patterns, which need *two* modulation vectors for their superspace description. These 2D pseudouniform arrangements appear in certain ranges of composition, and in some cases exhibit nano-chessboard-like features similar to those observed in the compounds mentioned at the beginning of this section. These patterns, resulting again from a basic drive to uniformity or maximal dilution within a lattice, involve a coherent arrangement of

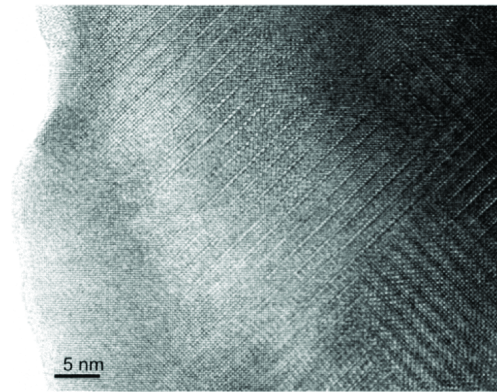


FIG. 2: HRTEM image of a striped ordering in $\text{Bi}_{1-x}\text{Ca}_x\text{FeO}_{3-x/2}$, $\sim 0.20 < x < \sim 0.49$, a perovskite-related phase viewed along an $[001]$ projection direction. Stripes of width $5a_p$ are realized for this particular grain (for details see Ref. 13).

structural motifs, which is rather different from the idea of ordered spinodal decomposition or phase segregation that has been previously proposed.

The paper is organized as follows. In Sec. II we review the basic ideas and results on pseudouniform stripe orderings in a simple two-dimensional $A_{1-x}B_x$ binary model presented recently (Ref. 17). In Sec. III we discuss the features and superspace description of a different family of pseudouniform $A_{1-x}B_x$ orderings which are intrinsically two-dimensional, including the determination of their two modulation vectors and their direct correspondence with the composition of the system. Finally, in Sec. IV we show how the above ideas can be useful to describe orderings in real systems.

II. PSEUDOUNIFORM 1D STRIPE COMPOSITIONAL ORDERING

The basic patterns appearing due to a drive to maximal dilution of minority motifs, abstracted from any other effects present in real systems, can be studied using a simple model of a square lattice with binary composition $A_{1-x}B_x$, in which the B “atoms” represent the minority motifs. In Ref. 17 the dilution drive was originally mimicked by isotropic Yukawa-type repulsive interactions between the B particles, and a simple lattice-gas simulated-annealing method was used to explore and generate pseudouniform patterns by minimizing the repulsion energy. For most compositions, stripe orderings of the type shown on Fig. 3 were found to optimize the lattice-ordered dilution of the B atoms. The stripes are formed by the concatenation of *tiles*, parallelepipeds delineated by B atoms, with a fixed composition and orientation within a stripe. For example, in Figure 3(a), the B atoms (the larger black dots) are present in the proportion $x=5/12$ and they achieve an ordered distribution as close as possible to uniformity by forming a

sequence of B -rich and B -poor stripes of tiles with composition $1/2$ and $1/3$ respectively (the smaller, square tile contains one A and one B atom, while the larger tile contains one B and two A atoms). As the overall B fraction $x=5/12$ is closer to $1/2$ than to $1/3$, the $1/2$ stripe regions are dominant (by a ratio 3:2), and the $1/3$ stripes have minimal width and are isolated, as if they could be considered minority motifs themselves, subject to a dilution drive. The fact that the stripe sequence and makeup follow strict rules as a function of overall composition was one of the main results of Ref. 17. The rules are based on the decomposition of the overall B fraction x in irreducible terms according to the Farey tree construction^{17,18}: for example, $x=5/12$ can be decomposed as $1/2 \oplus 1/2 \oplus 1/3 \oplus 1/2 \oplus 1/3$, where the \oplus notation indicates a simultaneous addition of numerator and denominator in the fractions (e.g. $n_1/m_1 \oplus n_2/m_2 = (n_1+n_2)/(m_1+m_2)$), which physically corresponds to the concatenation of two subsets of motifs of concentrations $x_1=n_1/m_1$ and $x_2=n_2/m_2$). This leads to the so-called uniform sequence [22323], which compactly indicates the composition and arrangement of the basic tiles in a pseudouniform stripe configuration.

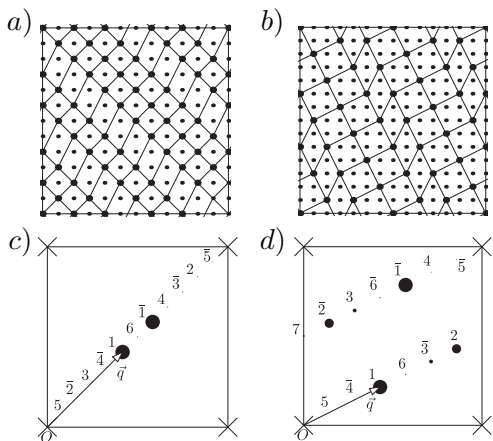


FIG. 3: Stripe orderings on a square lattice of composition $A_{1-x}B_x$ for $x = 5/12$ (a) and $x = 3/14$ (b), obtained via simulated-annealing optimization using an isotropic Yukawa-type repulsive interaction among the B atoms.¹⁷ (c) and (d): Fourier spectra (discs with radii proportional to the square modulus of the geometric structure factor) of the stripe arrangements shown in (a) and (b), showing the primary modulation wave vector. Only superstructure reflections are shown. The crosses indicate the reciprocal unit cell of the underlying square lattice. The superstructure reflections are indexed as satellite reflections according to the chosen primary modulation wave vector.

Figure 3(b) shows an analogous stripe ordering for $x=3/14$, where stripes with composition $1/5$ and $1/4$ are arranged according to the uniform sequence [554]. The stripe pseudouniform sequence corresponding to any other composition can be derived using the Farey tree construction. In most cases the arrangement involves ir-

reducible tiles of compositions $1/n$ and $1/(n+1)$ bracketing the overall B fraction x .¹⁷ These tiles can be seen as encoding at a local level the drive for dilution, and their overall arrangement according to the rules results in a pseudouniform intergrowth. As discussed in Ref. 17, the details of the repulsive model potential influence the details of the stability of different arrangements, so a purely repulsive criterion does not univocally lead to a single solution in two dimensions. Hence our consistent use of the term *pseudouniform* to refer to these orderings. Fine differences in stability are in practice irrelevant when one takes into account that the drive for dilution is a convenient but rough simplification of the state of affairs in real systems. This suggests that a fruitful approach to the problem of cataloging pseudouniform orderings in two dimensions is to abstract the basic ingredients, which are the irreducible, locally uniform, tiles, and their juxtaposition into intergrowth arrangements following appropriate rules.

Another key result of Ref. 17 is that the arrangements of the type shown in Figure 3 can be considered as compositionally modulated structures with a single composition-dependent primary modulation wave vector (a 1D modulation).¹⁷ The Fourier spectra (square modulus of the geometric structure factor) of these two examples are shown in Figure 3(c) and 3(d). One can see that the wave vectors $(5/12)(1,1)$ and $(3/14)(2,1)$, respectively, which are approximately orthogonal to the stripe direction, determine the location of the most intense *satellite* reflections stemming from the ordering. Within the superspace formalism originally developed to describe incommensurately modulated structures,^{19–21} these pseudouniform orderings can be described as long-period but commensurate structures with a simple step-like occupational modulation, with values either “atom A ” or “atom B ” in the relevant proportion, and using those vectors as primary modulation wave vectors. More specifically, a pseudouniform striped ordering is fully defined by an occupational modulation function $f(x_4)$ of period 1 with value “atom B ” in the interval $-x/2 < x_4 < x/2$ and value “atom A ” in the interval $x/2 < x_4 < 1 - x/2$ and a modulation vector \mathbf{q} that depends on x according to definite rules,¹⁷ such that the kind of atom occupying a site \mathbf{m} of the lattice is determined by the value of this function at $x_4=\mathbf{q}\cdot\mathbf{m}$. The continuous variable x_4 of the modulation function can be identified with the coordinate along the *internal space* used in the superspace formalism. Thus, when described by means of occupational modulations, pseudouniform orderings have their modulation functions reduced to simple consecutive A - and B -valued intervals (*atomic domains*) defined along the internal space in the superspace formalism.¹⁷

III. PSEUDOUNIFORM 2D COMPOSITIONAL ORDERING IN A PROTOTYPE $A_{1-x}B_x$ MODEL

A. The snub-square ordering

In some circumstances more complex, essentially two-dimensional, ordered configurations in the $A_{1-x}B_x$ system can become competitive and prevail (in the sense of maximal dilution) over the 1D striped arrangements studied in Ref. 17. For the case of a square lattice and an ideal isotropic dilution drive this happens for compositions within the interval $1/5 < x < 1/4$. This composition interval is special because the basic tiles corresponding to the compositions $x=1/4$ and $x=1/5$ can be juxtaposed with different orientations (the two sides of the two tiles have the same length), forming two-dimensional patterns (tilings). These 2D patterns were already considered in Ref. 22 in a simple context. Here we present a more complete picture of this family of orderings, their generating principles, and their description as modulated structures.

Simulations for the repulsive lattice-gas model mentioned in the previous section indeed confirm the apparition of intrinsically 2D ordered patterns in this composition range. Fig. 4 shows the ground states obtained for a composition $x=2/9$ for two different sizes of the simulation supercell (subject to periodic boundary conditions). The pseudouniform [45] stripe arrangement, in agreement with the rules explained in the previous section, was obtained for a minimal 9×9 supercell (Figure 4(b)). But for a 12×12 supercell, a completely different ordering pattern is stabilized (Figure 4(a)). It has the form of a so-called snub-square tiling²³ (with a slight modification: the rhombic $1/4$ tile can be considered formed by two triangles that are isosceles instead of being equilateral as in the canonical snub-square tessellation). This ordering pattern (henceforth SSQ ordering) prevails in the simulations over the stripe arrangement if the boundary conditions are compatible with both types of orderings.

A comparison of the distribution of B - B distances points to the main reason for the prevalence of the SSQ ordering over the striped one. As pointed out by Watson,²² both have the same distribution of B - B interatomic distances up to $\sqrt{10}$ (in cell parameter units of the underlying square lattice), but the SSQ ordering avoids the next distance $\sqrt{13}$ associated with neighbours separated by a vector $(3,2)$ or $(2,3)$, which is present in the striped arrangement.

Figure 4(c) and 4(d) presents sketches of the Fourier spectra of the SSQ ordering and of the competing striped arrangement. They clearly show the primary modulation wave vector(s) that can be identified in each case. The superstructure reflections of the striped arrangement can be indexed as linearly arranged satellites, with the strongest one being given by the modulation wave vector $\mathbf{q} = (2/9)(2,1)$, in accordance with the rules established in Ref. 17. The diffraction pattern of the SSQ ordering requires instead two primary wave vectors for a simple indexation of the satellite reflections, and the strongest

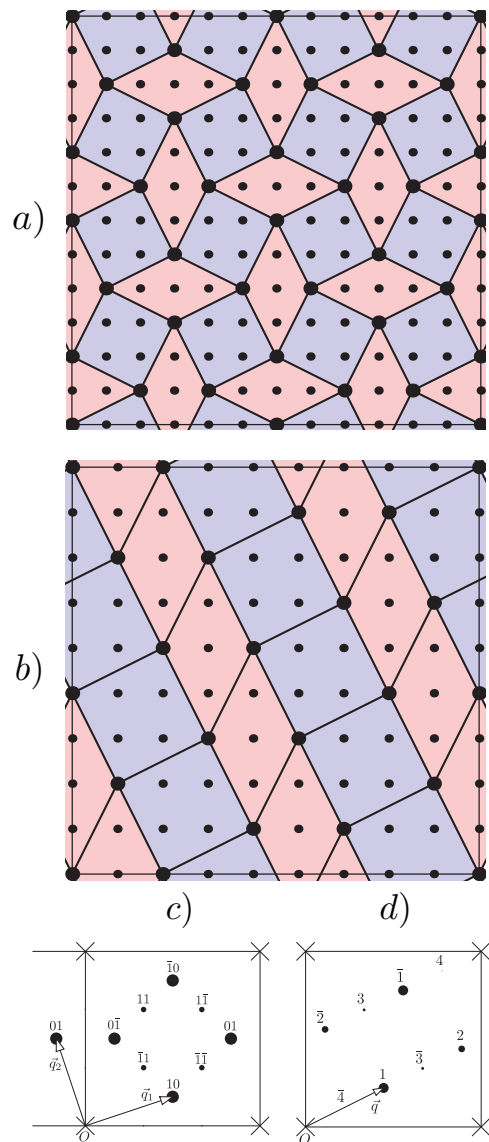


FIG. 4: Uniformity-driven orderings in a square lattice of composition $A_{1-x}B_x$ for $x=2/9$, obtained with simulations based on an isotropic Yukawa-type repulsive interaction among the minority B atoms, for 12×12 (a) and 9×9 (b) simulation boxes, and their corresponding Fourier spectra ((c) and (d)). The primary modulation wave vectors, one for the stripe arrangement (b) and two for the 2D tiling (a), are indicated in the corresponding Fourier diagram. The crosses in (c) and (d) indicate the reciprocal unit cell of the underlying square lattice. The superstructure reflections are indexed as satellites using the primary wave vector(s).

satellites indicate the most obvious choice: $\mathbf{q}_1 = (1/2, 1/6)$ and $\mathbf{q}_2 = (-1/6, 1/2)$.

The relevance of the SSQ-type arrangements as 2D orderings that could maximize somehow the uniformity of the distribution of a minority component for some specific compositions was pointed out in Ref. 22. We stress here that these configurations are indeed observed as

ground states in simulations of lattice gas models with repulsive interactions that mimic an isotropic drive to uniformity. In the following we will show their hierarchical structure when they are interpreted in terms of uniform sequences, and how they can produce nano-chessboard and nano-diamond patterns. In this framework, it will be shown that this type of arrangements, when described as compositional modulated structures, have some simple basic common ingredients which can be generalized and applied to explain and rationalize orderings in real systems generated at least in part by a drive to maximal uniformity, including ordered patterns in the nano scale.

B. Generalization of the snub-square ordering for any composition between 1/4 and 1/5.

The SSQ ordering for $x=2/9$ can be seen as a perfect array of intercrossing ribbons, each one formed by single tiles arranged in a $1/4 \oplus 1/5$ sequence. (From now on, to emphasize the actual arrangement of motifs in a sequence, we will use a slightly modified notation: $\{45\}$ indicates in this case an alternating sequence of 1/4 and 1/5 tiles, while the \square form will be reserved for pure numerical Farey term sequences for a specific concentration. In the stripe-ordering cases both notations are equivalent.) This topology, which avoids the distance $\sqrt{13}$ present in the stripe arrangement, can be generalized to any other composition in the interval $1/5 < x < 1/4$.²² For compositions different from 2/9, it is not possible to avoid the $\sqrt{13}$ distance completely, but in general the B - B distance distribution will still be favorable when compared to the stripe ordering. Following the argument in the previous section, we will discuss these generalized SSQ orderings in terms of our basic mechanism of juxtaposing appropriate tiles following certain rules, and we will not be concerned any more with detailed questions of maximal stability within a repulsive model. Figure 5(a) shows an example of a generalized SSQ ordering with $x < 2/9$. It corresponds to the case $x=9/41$, and is characterized by the crossing of two kinds of ribbons, one corresponding to the tile sequence $\{554\}$ (shown in the figure with shaded 1/5 tiles) and the other to the sequence $\{445\}$. In each ribbon, the minority tiles appear in a proportion 1/3, and the $\{445\}$ ribbons are also a minority in a proportion 1/3. The minority ratio 1/3 (which we will henceforth denote by α), is thus a key parameter in the construction of the pattern. In fact, if we take abstract motifs a and b , both the tile sequence in each ribbon and the ribbon arrangement sequence are instances of the physical sequence $\{aab\}$ (uniform sequence [3]), as befits a concentration $\alpha=1/3$. By comparison, for the SSQ ordering for $x=2/9$ in Figure 4(a), $\alpha=1/2$, which corresponds to a simple alternation of 1/4 and 1/5 tiles on each (identical) ribbon and a simple alternation in the ribbon arrangement (uniform sequence [2] for $\alpha=1/2$).

The parameter α fully characterizes the generalized SSQ orderings by determining the hierarchical tiling ar-

rangement, both at the level of each ribbon, and at the level of ribbon kinds. As it relates to a minority concentration, we can take without loss of generality $\alpha \leq 1/2$, and the general relation between α and x is given by:²²

$$x = \frac{2}{9 \pm (1 - 2\alpha)^2} \quad (1)$$

where the plus sign in the denominator corresponds to $1/5 < x < 2/9$ (with 1/4 tiles underrepresented), and the minus sign to $2/9 < x < 1/4$ (with relative abundance of 1/4 tiles).

Fig. 5(b) shows the corresponding arrangement for a composition much closer to 1/5, $\alpha=1/9$ ($x=81/389=0.20826$). This ordering optimizes the distribution of B - B interatomic distances towards larger values by forming large squares of composition $x=1/5$, separated by single ribbons with an inverted 1/9 proportion of 1/5 tiles, in an effective sequence $\{44444445\}$. Despite the large size of the square blocks, the system cannot be considered subject to phase segregation. On the contrary, the regions with different local composition are coherently interleaved and ordered as a single phase. Paradoxically, it is the quest for uniformity that can drive the system into this type of chessboard orderings. For α values of type n/m , the patterns become more complex, as the ribbons with a proportion n/m of basic tiles of type either 1/4 or 1/5 must be ordered according to a 1D non trivial pseudouniform sequence of the type explained in the previous section. The presence of 1D uniform sequences (derived from the Farey-tree construction) along the individual ribbons is in fact the signature that the ordering is being driven by a uniformity quest. Figure 6 shows two examples for $\alpha=2/7$ and $3/7$. One can see in this figure that a more complex uniform sequence is realized in the way the 1/4 and 1/5 basic tiles are arranged along each oblique ribbon, with either 1/4 or 1/5 tiles as minority in a proportion α . For $\alpha=2/7$ ($=1/3 \oplus 1/4$), the relevant abstract uniform sequence is $\{aabaab\}$ ([34]), leading to interlocking ribbons of the form $\{4454445\}$ and $\{5545554\}$, which themselves are in a proportion 2/7 with the same sequencing.

For a rational value of x , the corresponding α according to Eq. (1) is in most cases irrational, and therefore the generalized SSQ ordering for that x is incommensurate with respect to the underlying lattice. The ribbons of basic tiles will follow an aperiodic uniform sequence corresponding to the irrational value of α , still according to the Farey tree construction.¹⁷ Thus, the tendency to uniformity could conceivably stabilize 2D incommensurate orderings of minority motifs even if their proportion is a simple rational value. For instance, the generalized SSQ ordering for $x=3/14$, which competes with the stripe arrangement shown in Figure 3(b), would be an incommensurate ordering with α having an irrational value close to 2/9.

Within the interval $2/9 < x < 1/4$ the number of 1/4 tiles is larger than that of 1/5 tiles, and the ordering patterns follow then the same rules but with the roles of

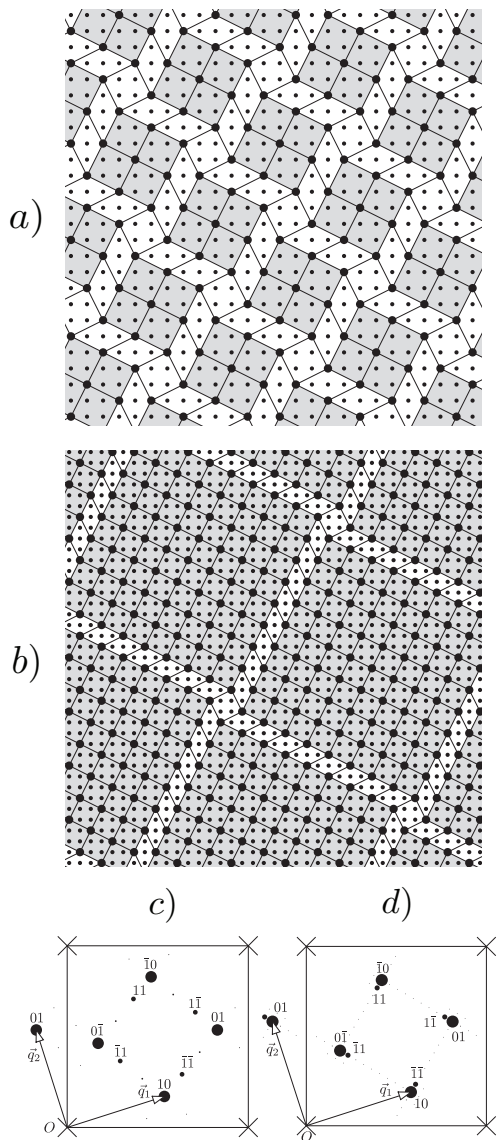


FIG. 5: Generalized snub square orderings in a square lattice of composition $A_{1-x}B_x$ for (a) $x=9/41=0.219512$ ($\alpha=1/3$) and (b) $x=81/389=0.20826$ ($\alpha=1/9$) and their corresponding Fourier spectra ((c) and (d)). The crosses in (c) and (d) indicate the reciprocal unit cell of the underlying square lattice. The superstructure reflections are indexed as satellites using the primary wave vectors that are indicated.

the two types of basic tiles interchanged, such that the ribbons having a proportion α of $1/5$ tiles become majority. As x approaches the composition limit $x=1/4$, blocks of density $1/4$ increase in size, forming patchwork patterns of diamond shape, as shown in Fig. 7.

We see that the α parameter acts as an auxiliary “minority concentration”, controlling the arrangement of the $1/4$ and $1/5$ basic tiles, which in themselves encapsulate a maximal local uniform ordering. The only other essential ingredient that makes the SSQs orderings more uniform than the stripe arrangements for the same composition is

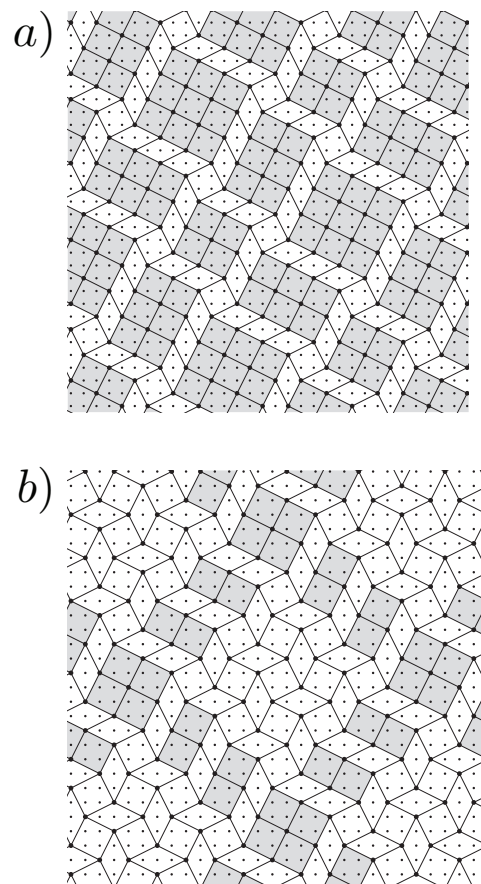


FIG. 6: Generalized snub square orderings in a square lattice of composition $A_{1-x}B_x$ for (a) $x=49/225=0.217778$ ($\alpha=2/7$) and (b) $x=49/221=0.221719$ ($\alpha=3/7$)

the intercrossing feature that tends to eliminate as much as possible the $\sqrt{13}$ distance.

C. Description of uniformity-driven 2D orderings as modulated structures

Although the generalized SSQ orderings discussed above present a large variety of arrangements, their diffraction patterns are very similar. They exhibit a strong hierarchy in the intensity of the superstructure reflections, characteristic of modulated structures (see Figures 4, 5, and 7). The strongest superstructure reflections can be taken as first-order satellites, and define the primary modulation vectors, while the remaining ones can be indexed as higher-order satellites. In Section III A we showed the primary modulation wave vectors that can be associated with the $x=2/9$ SSQ ordering. These are particular values among those that can be obtained for generalized SSQ arrangements, which depend on the composition according to simple rules of geometrical origin. In Figure 5c), for example, the second-order satellite

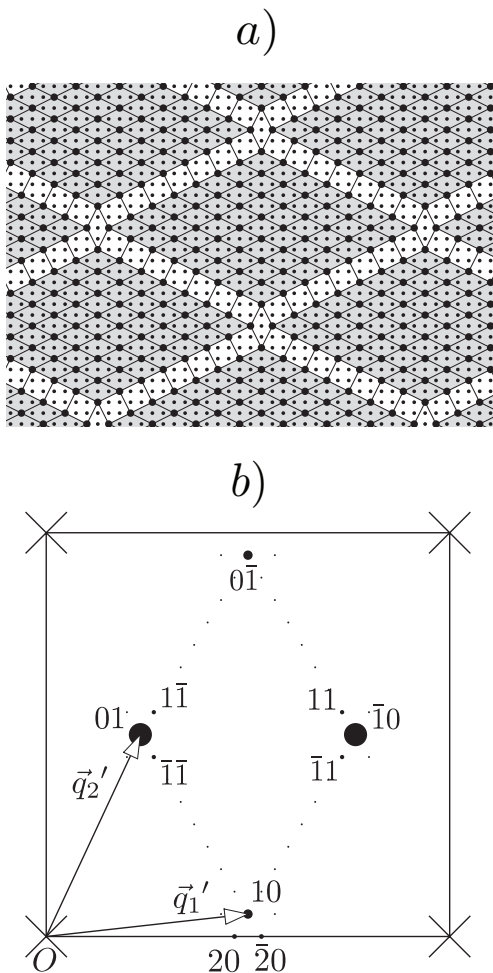


FIG. 7: (a) Generalized snub square orderings in a square lattice of composition $A_{1-x}B_x$ for $x=32/135=0.237037$ ($\alpha=1/8$, $x > 2/9$) and (b) sketch of its Fourier spectrum. Superstructure reflections are indexed as satellites with primary modulation vectors \mathbf{q}'_1 and \mathbf{q}'_2 (which in this case, as $x > 2/9$, do not follow Eqs. 2)

($\bar{1}\bar{1}$) lies along the line joining two first-order satellites, and at distances from them which are fractions α and $1 - \alpha$ of the length of the line. This constraint, together with a simple symmetry argument (existence of a symmetry plane for $x > 2/9$, and tetragonality for $x < 2/9$), is enough to fix the modulation vectors. To be short, we only describe those corresponding to the cases with $1/5 < x < 2/9$. In this interval, the two modulation wave vectors are given by the equations:

$$\begin{aligned} \mathbf{q}_1 &= \left(\frac{1}{2} - \frac{x(1-2\alpha)}{2}, \frac{1}{2} - \frac{3x}{2} \right) \\ \mathbf{q}_2 &= \left(-\frac{1}{2} + \frac{3x}{2}, \frac{1}{2} + \frac{x(1-2\alpha)}{2} \right) \end{aligned} \quad (2)$$

and are an explicitly tetragonal and right-handed set, best suited for the construction of the superspace model to follow. (There is an alternate choice of modulation

vectors $\mathbf{k}_1 = \mathbf{q}_1$ and $\mathbf{k}_2 = (1, 0) - \mathbf{q}_2$, with the extra property that $|\mathbf{k}_1 \times \mathbf{k}_2| = x$. Also, these “natural” vectors are reciprocal to the real space vectors defining a “virtual” monatomic unit cell that best approximates the uniform motif distribution with density x (in correspondence with the concept described in Ref. 17).)

The SSQ ordering can now be described as a modulated structure with the modulation vectors of Eqs. 2 and with an occupational modulation defined by a function $f(x_4, x_5)$, of period 1 for both variables, such that the atom occupying a given lattice site $\mathbf{m} = (m_1, m_2)$ is determined by the value (either “atom A” or “atom B”) of $f(x_4, x_5)$ for $x_4 = \mathbf{q}_1 \cdot \mathbf{m}$ and $x_5 = \mathbf{q}_2 \cdot \mathbf{m}$. Maps of the function $f(x_4, x_5)$ sampled at the discrete values of x_4 and x_5 that correspond to the SSQ orderings considered so far are shown in Figure 8. As it happens in the 1D case, the domain with value “atom B”, corresponding to the minority motifs, forms a single compact/dense region with an area equal to their proportion x in the lattice. Thus the minority atoms B aggregate in the internal space of the occupational modulation function in order to describe arrangements in which these atoms are maximally scattered in real space. (As remarked above, for irrational α one would obtain from Eqs. 2 incommensurate wave vectors, and the sampling of the A - and B -valued domains would be continuous.) The B atomic domains have in all cases a form which avoids the occupation by B atoms of two neighbouring lattice sites. This restriction is ensured by the geometrical condition shown in Figure 8: The B atomic domains, if translated on the plane (x_4, x_5) by either $(\mathbf{q}_1 \cdot (1, 0), \mathbf{q}_2 \cdot (1, 0))$ or $(\mathbf{q}_1 \cdot (0, 1), \mathbf{q}_2 \cdot (0, 1))$, juxtapose with the original one, with no superposition. Within the superspace formalism this is termed “closeness condition”, and is known to be satisfied by the atomic domains describing some quasicrystals.^{24,25} The atomic domain borders can be taken parallel to the basis vectors of the point lattice in internal space formed by the points $(\mathbf{q}_1 \cdot \mathbf{m}, \mathbf{q}_2 \cdot \mathbf{m})$, where \mathbf{m} represents the direct lattice points. This, together with the closeness condition and Eqs. 2, is sufficient to define the appropriate atomic domain B for any composition x , and to construct with it its corresponding SSQ ordering.

IV. UNIFORMITY-DRIVEN ORDERINGS IN REAL SYSTEMS

We have considered above an idealized $A_{1-x}B_x$ model for which the optimal ordering within a lattice depends only on the maximization of the dilution of minority motifs. In real systems this factor can be one among many others. For instance, intrinsic anisotropies of the underlying crystalline lattice, energy constraints on possible orderings (for instance, compatibility with rigid unit modes, chemically forbidden geometries, etc.) can play a fundamental role in favoring a particular ordering pattern. Nevertheless, if an effective dilution still retains a main role in these realistic scenarios, some of the fea-

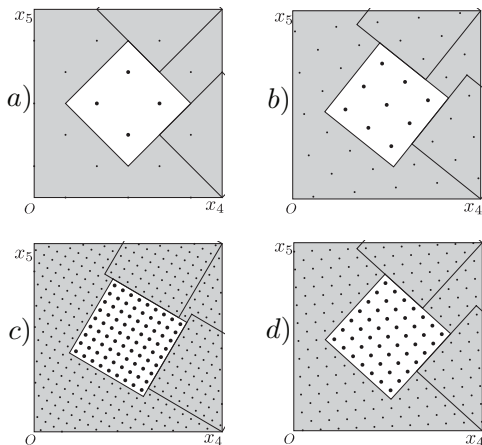


FIG. 8: Maps of the occupational step-like modulation functions $f(x_4, x_5)$ that describe, taking as modulation wave vectors the vectors \mathbf{q}_1 and \mathbf{q}_2 of Eqs. 2, the generalized snub square orderings for $x=2/9$ (a), $9/41$ (b), $81/389$ (c) and $49/221$ (d), which are shown in Figures 4,5, and 6, respectively. The (x_4, x_5) coordinates of B -occupation sites are indicated with larger dots, and A -sites with smaller ones. The A (dark) and B -valued (clear) domains of the simplest function consistent with the occupied A and B sites are indicated in each case. A single unit cell of the internal space is shown. The closeness condition satisfied by the neighboring B -valued domains in the superspace description is shown by means of continuous lines corresponding to their projected borders.

tures of the purely uniformity-driven orderings are very likely to be maintained. One of the features which are present in the above discussion is the possibility of constructing the orderings through the juxtaposition (intergrowth) of basic tiles. These encapsulate at the local level the drive for dilution, and their combination, as we have seen, can lead to a variety of patterns, depending on the geometrical flexibility involved. Fig. 9(a) shows a sketch of the ordering pattern of oxygen vacancies observed in layers of the compounds $\text{La}_{8-x}\text{Sr}_x\text{Cu}_8\text{O}_{20-\delta}$, $(\text{La}, \text{Sr})_8\text{Cu}_8\text{O}_{18}$ and $\text{La}_2\text{Sr}_6\text{Cu}_8\text{O}_{16}$.²⁶ To our knowledge, this is the first time that this ordering is interpreted as a tiling, similar to the SSQ, but with tiles of composition $1/3$ and $1/5$, so that the global vacancy density is $1/4$. In this case the ordering is not optimizing a purely repulsive interaction (which would lead for this composition to a monatomic superlattice of vacancies), but the drive for dilution is still obviously present. Considered as an abstract geometrical and numerical exercise, the combination rules for the $1/3$ and $1/5$ tiles lead to the same kind of regularities discussed above for the $1/5$, $1/4$ tiles, including the appearance of coherent generalized nanopatches (nano-rhombi in this case).²⁷ Crucially, all the arrangements produced through the $1/5$ - $1/3$ tile combinations are also describable as occupationally modulated structures, with compact atomic domains in the superspace construction, and with modulation vectors that can

be read directly from the diffraction diagram. For the case of the vacancy distribution in Fig. 9(a), the primary modulation wave vectors can be chosen as $\mathbf{q}_1=(1/2, 1/4)$ and $\mathbf{q}_2=(-1/4, 1/2)$, as seen in the diffraction diagram of Fig. 9(b), and the corresponding modulation function is shown in Figure 9(c). The four independent vacancies within the 16 atomic sites form again a single simple atomic domain fulfilling the closeness condition described above.

Once again we see that the ordered patterns are describable as modulated phases with step-like modulation functions, with the B -valued regions of the functions limited to one or a few domains within the unit-cell of the periodic function, and with the fulfilment of some kind of closeness condition. Modulated structures with modulation functions of this type are very efficient for distributing regularly minority motifs in real space. With all the evidence presented so far (here and in the previous work over several years)^{9,28-32} we can say that in a real system the knowledge of the relevant modulation vectors (extracted from its diffraction diagram) is sufficient to design, through the rules explained above, a compositionally modulated model which corresponds to an atomic ordering with a high degree of uniformity in the distribution of some specific motif. Thus we can postulate an atomic distribution model with a specific composition and a maximal dilution consistent with the observed modulation vectors. If a drive for dilution is at work, this a priori model should approximate the experimental arrangement. This clearly occurs in the example shown in Fig. 9, and also seems to happen in the nano-chessboard arrangements observed in the compounds mentioned in the introduction. As shown below, the basic features of the latter can be reproduced in a simplified binary system by postulating a compositionally modulated arrangement with step-like atomic domains that fulfill the closeness condition, and are consistent with the observed modulation vectors. This would indicate that the observed arrangements represent some optimization of the dilution of the atoms within the underlying perovskite lattice, but subject to some anisotropic constraints that force the possible modulation vectors.

Let us consider for instance the compound $\text{Li}_{1/2-3y}\text{Nd}_{1/2+y}\text{TiO}_3$ mentioned in the introduction. Figure 10 shows a $[001]$ zone electron diffraction pattern (EDP) of this material with $y=0.067$ (we change the letter for the composition variable to avoid confusion with that employed in our binary toy model). The primary modulation wave vectors can be identified directly from the EDP diagram as $\mathbf{q}_1=(1/2-\epsilon, -1/2)$ and $\mathbf{q}_2=(1/2, 1/2-\epsilon)$ with ϵ about $1/30$. One cannot pretend to derive from this information a quantitative structural modelling of this compound, but we can determine for our simple 2D $A_{1-x}B_x$ binary system a pseudouniform ordering of the B atoms consistent with these modulation vectors. Using the rules explained above, we have to consider an occupational modulation function $f(x_4, x_5)$ fulfilling the closeness condition for these modulation

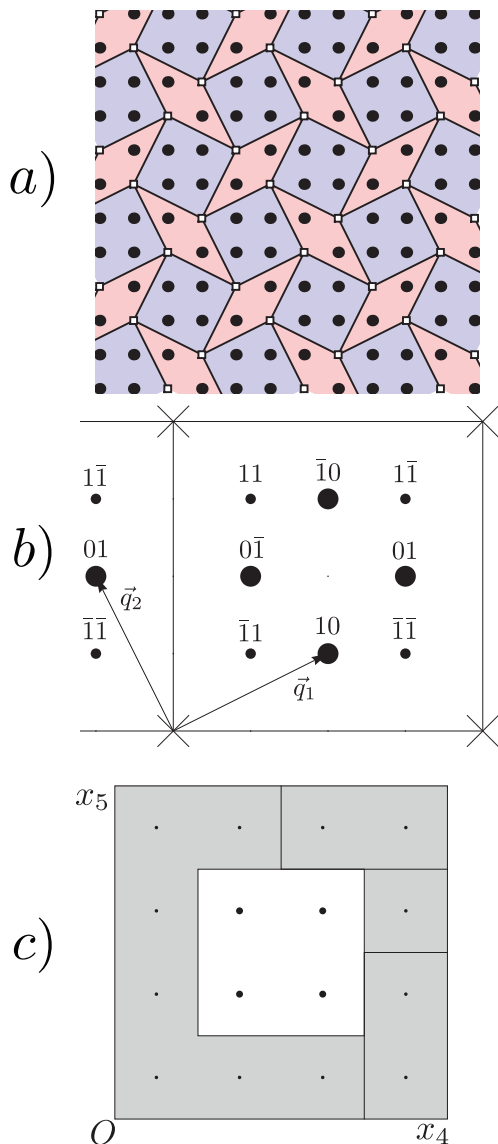


FIG. 9: (a) Ordering pattern of the oxygen vacancies reported in the layers $\text{BO}_{2-\delta}$ of $\text{La}_{8-x}\text{Sr}_x\text{Cu}_8\text{O}_{20-\delta}$, $(\text{La},\text{Sr})_8\text{Cu}_8\text{O}_{18}$, and $\text{La}_2\text{Sr}_6\text{Cu}_8\text{O}_{16}$ (Ref. 26), interpreted as a $1/3\oplus 1/5$ tiling in a virtual square lattice in which vacancies are present in a proportion $x=1/4$. (b) Diffraction diagram showing the modulation vectors $\mathbf{q}_1=(1/2,1/4)$ and $\mathbf{q}_2=(-1/4,1/2)$ that index the satellites. (c) Map of the modulation function that can be associated with the ordering pattern using \mathbf{q}_1 and \mathbf{q}_2 (symbols and extra closeness-condition lines as in Figure 8).

vectors. This simple step-like occupational modulation function (see Fig. 11(b)), yields the atom ordering shown in Fig. 11(a), which vividly recalls the nano-chessboard arrangements observed in this compound. The square patches have composition AB, while the global excess of A atoms are localized at the interfaces, which are made only of A atoms and are limited to two unit cells of the underlying lattice. By construction, the composition

of this $A_{1-x}B_x$ nano-chessboard arrangement is fully determined by the modulation vectors, and is given by the relative area of the B atomic domain in Fig. 11(b), which is $x=1/2-\epsilon+\epsilon^2$, i.e. $x=421/900=0.467778$. Obviously this composition is not comparable with that of $\text{Li}_{1/2-3y}\text{Nd}_{1/2+y}\text{TiO}_3$. The arrangement of Fig. 11 is far from the real system, not only due to the reduction to a 2D $A_{1-x}B_x$ arrangement, but also because the vacancies accompanying the Nd/Li substitution and the expected very large positional relaxations are ignored. But nevertheless, this simple occupational modulation with an intrinsic tendency to uniformity and consistent with its modulation vectors in a binary system, is sufficient to reproduce basic features of the real system. Notice for instance the shift of the A and B occupation sites in contiguous patches of composition $A_{1/2}B_{1/2}$ of the chessboard, as proposed in the model for $\text{Li}_{1/2-3y}\text{Nd}_{1/2+y}\text{TiO}_3$ of Ref. 1. Fig. 11(c) shows the geometric diffraction pattern of this 2D $A_{1-x}B_x$ nano-chessboard arrangement. It is remarkable that despite the strong anharmonicity of the occupational modulation only odd-order satellites are observable. This is consistent with the Fourier decomposition of the underlying two dimensional step-like occupational modulation. In the real system even-order satellites close to the main reflections are also significant, which is probably due to the strong displacive modulations in the perovskite framework (mainly tiltings), induced by the cation ordering. This can be a plausible explanation, since by just introducing a small displacive sinusoidal modulation with wave vectors $\mathbf{q}_1+\mathbf{q}_2$ and $\mathbf{q}_1-\mathbf{q}_2$ of the A and B positions in the configuration of Fig. 11(a), we can produce a diffraction diagram similar to the experimental one of Figure 10.

Nano-chessboards of the type reported in Refs. 1–3 may therefore originate in a drive for maximal uniformity in the distribution of a minority motif. If this were indeed the mechanism, the width of the interface regions between the chessboard patches, although clearly wider than in our model due to structural displacive relaxations, should be independent of the size of the patches, i.e. of the system composition. A careful check of the fulfillment or not of this property by the nano-chessboards observed in real systems would be a key feature for the validation of a uniformity-drive mechanism.

V. CONCLUSIONS

We have shown that a drive towards dilution of minority structural motifs constrained to an underlying lattice is sufficient to produce two-dimensional orderings with local composition variations in the nanoscale. The dilution can be achieved in practice by the combination or intergrowth of basic tiles that encapsulate a local repulsion of minority motifs. This combination principle is able to generate orderings that are hierarchically structured, adopting for certain compositions the form of

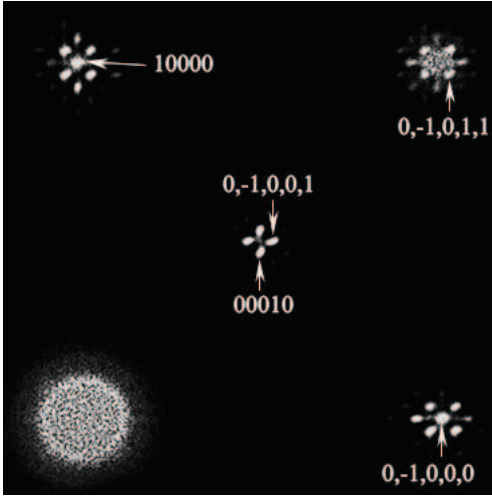


FIG. 10: [001] zone electron diffraction pattern of the (3+2)-D incommensurately modulated, nano chessboard phase of $\text{Li}_{0.30}\text{Nd}_{0.567}\text{TiO}_3$, indexed with respect to the basis set $\mathbf{M}^* = \{ \mathbf{a}^* = \mathbf{a}_p^*, \mathbf{b}^* = \mathbf{b}_p^*, \mathbf{c}^* = 1/2\mathbf{c}_p^*, \mathbf{q}_1 = 1/2\mathbf{a}_p^* + (1/2-\epsilon)\mathbf{b}_p^*, \mathbf{q}_2 = (-1/2+\epsilon)\mathbf{a}_p^* + 1/2\mathbf{b}_p^* \}$, where the subscript p stands for parent perovskite, and $\epsilon \sim 1/30$.

nano-chessboards or diamond-like patches. In all cases, regions of two different effective compositions are interleaved coherently, with long-range order.

The mechanism leading to composition patterning from a dilution drive has already been documented in other systems: layer arrangement in compositionally flexible layered compounds,^{9,28-32} and two-dimensional systems exhibiting effectively 1D stripe patterns.¹⁷ Here we find what appears to be a segregation of phases instead of a pseudouniform distribution, but these arrangements are in fact near-optimally uniform by any reasonable criterion, and their underlying structure (now essentially two-dimensional instead of effectively 1D) can be described by the same recipe at work in the pseudouniform systems previously studied: modulation vectors directly and simply determined from the intensity distribution in the diffraction diagram, and step-like occupational modulations satisfying a closeness condition for these modulation vectors.

The description in terms of occupational modulations, best represented using the tools of the superspace formalism, is thus seen as the unifying structural principle in a wide variety of systems which exhibit in some degree a dilution drive. The key idea is that minority motifs maximally scattered in real space are represented by compact regions in the internal coordinates of the superspace construction.

We have shown that this powerful principle seems to be at work for two kinds of relevant experimental systems. In the case of the distribution of vacancies in $\text{La}_{8-x}\text{Sr}_x\text{Cu}_8\text{O}_{20-\delta}$, $(\text{La},\text{Sr})_8\text{Cu}_8\text{O}_{18}$ and $\text{La}_2\text{Sr}_6\text{Cu}_8\text{O}_{16}$,²⁶ the resulting pattern can be seen also as a direct example of the tiling rules in real space.

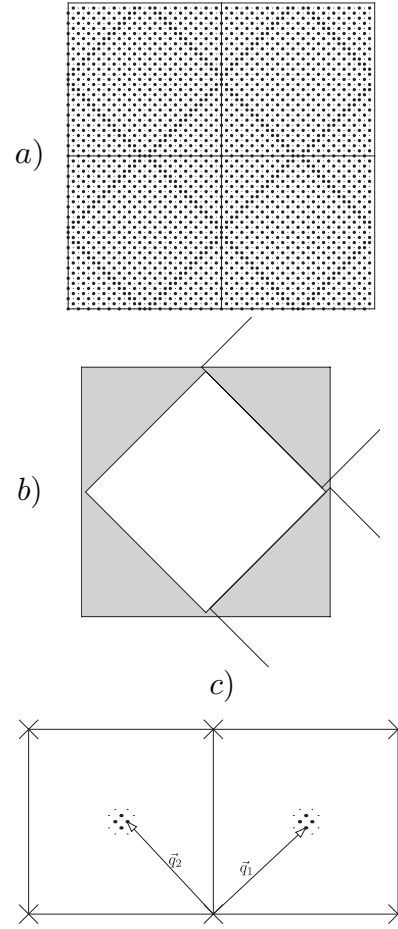


FIG. 11: (a) Chessboard nanopattern in a square lattice of composition $A_{1-x}B_x$, obtained as a compositionally modulated structure with modulation wave vectors $\mathbf{q}_1 = (1/2, 1/2 - \epsilon)$ and $\mathbf{q}_2 = (-1/2 + \epsilon, 1/2)$ with $\epsilon = 1/30$ (i.e. those present in $\text{Li}_{1/2-3y}\text{Nd}_{1/2+y}\text{TiO}_3$), and a step-like A/B occupational modulation function fully determined by the closeness condition of the B domains for these modulation vectors. This modulation function is shown in (b), where A and B -valued domains are depicted as dark and clear regions, respectively, within a 2D period of the function (i.e. a unit cell of the internal space in the superspace construction). The closeness condition satisfied by the neighboring B -valued domains in the superspace description is shown by means of continuous lines corresponding to their projected borders. The corresponding geometric diffraction pattern is shown in (c).

The nano-chessboard arrays, and similar patterns exhibiting composition patterning, that have been recently observed in composition flexible systems such as $\text{Li}_{1/2-3x}\text{Nd}_{1/2+x}\text{TiO}_3$ are strongly reminiscent of the kinds of hierarchical real-space orderings that appear in uniformity-driven simple models. They reproduce basic features of the observed nano-chessboard arrangements, and their Fourier spectra exhibit the kind of strong hierarchical satellite structure present in the experimental diffraction diagrams. We can thus suggest that the ob-

served compositional changes at the nanoscale in these compounds have their origin, at least partially, in a drive for uniformity, maintaining the coherency of a single phase, and are not, as previously proposed, due to any kind of phase separation.

Acknowledgements

This work has been supported by the Spanish Ministry of Science and Innovation (projects MAT2008-05839

and FIS2009-12721-C04-O3) and by the Basque Government (project IT-282-07). Technical and human support provided by IZO-SGI SGIker (UPV/EHU, MICINN, GV/EJ, ERDF, ESF) is gratefully acknowledged. RLW acknowledges financial support from the Australian Research Council in the form of ARC Discovery Grants.

-
- * Electronic address: wmpemam@ehu.es
- ¹ B. Guiton and P. K. Davies, *Nature Materials* **6**, 586 (2007).
 - ² S. Garcia-Martin, G. King, E. Urones-Garrote, G. Nenert, and P. M. Woodward, *Chem. Materials* **23**, 163 (2011).
 - ³ M. W. Licurse, A. Y. Borisevich, and P. K. Davies, *Journal of Solid State Chemistry* **191**, 220 (2012).
 - ⁴ K. Schubert, B. Keifer, M. Wilkens, and R. Kaufler, *Z. Metallkde.* **46**, 692 (1955).
 - ⁵ O. Terasaki and D. Watanabe, *Jpn. Jnl. Of Appl. Phys.* **10**, 292 (1971).
 - ⁶ D. Watanabe and K. Takashima, *J. Appl. Cryst.* **8**, 598 (1975).
 - ⁷ L. A. Bursill and B. G. Hyde, *Acta Cryst. B* **27**, 210 (1971).
 - ⁸ L. A. Bursill, *Proc. Roy. Soc. Series A* **311**, 267 (1969).
 - ⁹ L. Elcoro, J. M. Perez-Mato, and R. Withers, *Z. Kristallogr.* **215**, 727 (2000).
 - ¹⁰ S. Schmid, J. G. Thompson, A. D. Rae, B. D. Butler, R. L. Withers, N. Ishizawa, and S. Kishimoto, *Acta Cryst. B* **51**, 698 (1995).
 - ¹¹ A. D. Rae, S. Schmid, J. G. Thompson, R. L. Withers, and N. Ishizawa, *Acta Cryst. B* **51**, 709 (1995).
 - ¹² Y. Michiue, A. Yamamoto, M. Onoda, A. Sato, T. Akashi, H. Yamane, and T. Goto, *Acta Cryst. B* **61**, 145 (2005).
 - ¹³ J. Schiemer, R. Withers, L. Noren, Y. Liu, L. Bourgeois, and G. Stewart, *Chem. Mater.* **21**, 4223 (2009).
 - ¹⁴ A. Janner and T. Janssen, *Acta Cryst. A* **36**, 399 (1980).
 - ¹⁵ A. Janner and T. Janssen, *Acta Cryst. A* **36**, 408 (1980).
 - ¹⁶ P. M. de Wolf, *Acta Cryst. A* **30**, 777 (1974).
 - ¹⁷ S. González, J. M. Perez-Mato, L. Elcoro, and A. Garcia, *Phys. Rev. B* **84**, 184106 (2011).
 - ¹⁸ J. Farey, *Philosophical Magazine* **47**, 385 (1816).
 - ¹⁹ T. Janssen, G. Chapuis, and M. de Boissieu, *From modulated phases to quasicrystals* (Oxford University Press, 2007).
 - ²⁰ T. Janssen, A. Janner, A. Looijenga-Vos, and P. M. de Wolf, *International Tables for Crystallography C, A.J.C. Wilson Ed., p 797-835* (Kluwer Academic Publishers, 1992).
 - ²¹ S. van Smaalen, *Incommensurate crystallography* (Oxford University Press, 2007).
 - ²² G. I. Watson, *Physica A: Statistical and Theoretical Physics* **246**, 253 (1997).
 - ²³ B. Grünbaum and G. C. Shephard, *Tilings and Patterns* (New York: W.H. Freeman, 1987).
 - ²⁴ M. Cornier-Quiquandon, D. Gratias, and A. Katz, *Methods of Structural Analysis of modulated Structures and Quasicrystals. J. M Perez-Mato, F.J. Zúñiga, G. Madariaga Eds., p 313-332* (World Scientific, 1992).
 - ²⁵ A. Katz and D. Gratias, *J. Non Crystalline Solids* **153-154**, 187 (1993).
 - ²⁶ J. Hadermann, G. V. Tendeloo, and A. M. Abakumov, *Acta Cryst. A* **61**, 77 (2005).
 - ²⁷ S. González, J. M. Perez-Mato, and L. Elcoro, (unpublished) (2011).
 - ²⁸ J. M. Perez-Mato, M. Zakhour-Nakhl, F. Weill, and J. Darriet, *J. Mater. Chem.* **9**, 2795 (1999).
 - ²⁹ P. Boullay, G. Trolliard, D. Mercurio, J. M. Perez-Mato, and L. Elcoro, *J. Solid State Chem.* **164**, 252 (2002).
 - ³⁰ J. Darriet, L. Elcoro, A. E. Abed, E. Gaudin, and J. M. Perez-Mato, *Chem. Mater.* **14**, 3349 (2002).
 - ³¹ Y. Michiue, A. Yamamoto, and M. Tanaka, *Acta Cryst. B* **62**, 737 (2006).
 - ³² Z. Izaola, S. Gonzalez, L. Elcoro, J. M. Perez-Mato, G. Madariaga, and A. Garcia, *Acta Cryst. B* **63**, 693 (2007).